

# PROJECT REPORT

---

## Semantic Segmentation of Wounds

---

**Cay Rahn**  
6255648

**Course:** KEN4244 Deep Learning for Image & Video Processing  
**Academic Year:** 2023/24

December 18, 2023

# 1 Introduction

## 1.1 Motivation

- many people affected by chronic wounds that need to be monitored
- Why is automatic Wound Segmentation so important? And why is it a complex problem?
- Manual segmentation by experts expensive and very time consuming
- experts differ in their segmentation
- different types of wounds have different characteristics
- changing lighting conditions, distance to camera, camera angle, different cameras have impact on result
- controlled environment not feasible in clinical setting
- ideally, we want to be able to take pictures with a smartphone without overly complicated instructions for the person taking the picture
- experience as photographer should not be required, clinical professionals should be able to take pictures that are then segmented correctly
- one type: diabetic foot ulcers → are monitored to ensure healing process is optimal and there is no infection, normally long time span [12]
- wounds have complex structure containing different types of tissue with different colour and texture → different regions with borders in between [1]
- heterogeneous wound images

## 1.2 Research Questions

A recent publication by Oota et al. claims to have improved the state of the art in the field of Wound Segmentation. Such claims always need to be supported by further research. This project aims to investigate and reimplement the proposed method. Furthermore, the method is set into context with state-of-the-art methods for semantic segmentation in general and for wounds specifically.

- can the results be reproduced?
- what influence does the input image size have? Can we rescale the images and are able to transfer what is learned
- how robust is the model/architectures to transformations/distortions on the input
- XAI

# 2 Datasets

Unfortunately, few datasets on chronic wounds are publicly available [20]. They often feature only a specific type of chronic wound, mainly diabetic or pressure ulcer. An example of such a specialised dataset is the data from the Diabetic Foot Ulcer Challenge 2022 [12]. However, it is only available after application and, therefore, is inappropriate for this project due to its limited timescope. Another data set featuring foot ulcer wounds is publicly available in the Foot Ulcer Segmentation Challenge

2021 [23]. It consists of 1010 images, which are augmented to build a data set with a training set of 3645 images and a test set of 405 images. Due to the nature of the challenge, labels for the test set are unavailable.

**WSNet data set** The data set mainly used in the scope of this project is the WSNet data set featuring eight different wound types: venous ulcer, trauma wound, diabetic ulcer, surgical wound, arterial ulcer, cellulitis, pressure ulcer and a not further specified group of other wounds [20, 19]. In total, it consists of 2686 images and their corresponding masks. With this, it consists of more individual images and wound types than the publicly available data set mentioned above. Unfortunately, the wound classification itself is not available. Furthermore, Oota et al. mention another separate data set for pre-training with wound type classification, which is also not publicly available.

### 3 State of the Art

#### 3.1 Semantic Segmentation

The segmentation of wounds belongs to the class of semantic segmentation problems, where a pixel-wise classification is performed. In the case of wound segmentation, there are two classes: foreground, which is the wound, and background. Deep Learning methods have become dominant in the last few years because they have become more accessible. Fully Convolutional Neural Networks (fCNN) as a starting point in research had the drawback of resulting in a low output resolution, and multiple techniques were invented to increase the output resolution [15]. This results in an encoder-decoder architecture as the base for the networks, inspired by auto-encoders [4], where the encoder subsamples and the decoder upsamples [18]. In such architectures, the encoder generates context information, information in the feature space, while the decoder maps this information into the spatial context.

Pre-training for such models requires a vast amount of data. The typical object classification data set for such pre-training is the ImageNet data set [2].

This project uses four segmentation models: U-Net, LinkNet, FPN and PSPNet. All are improved architectures about a basic fCNN. Each architecture is described in detail to understand the challenges and approaches to localising information in space.

**U-Net** U-Net is a convolutional network developed for biomedical image segmentation based on an encoder-decoder architecture. Encoder and decoder are called contracting and expansive paths in the original paper, describing their function. They are also described as context and spatial paths [17]. Both the encoder and decoder consist of different steps to encode and decode the image on different spatial levels. The encoder is a classical CNN; each step consists of two convolutions and a max pooling operation for downsampling. The decoder step upsamples the feature map followed by a convolution. The result is then concatenated with the corresponding feature map from the encoder path, and convolution is applied again. In the final layer, 1x1 convolution maps the feature vector to the desired number of classes. This architecture is visualised in Figure 1. [21]

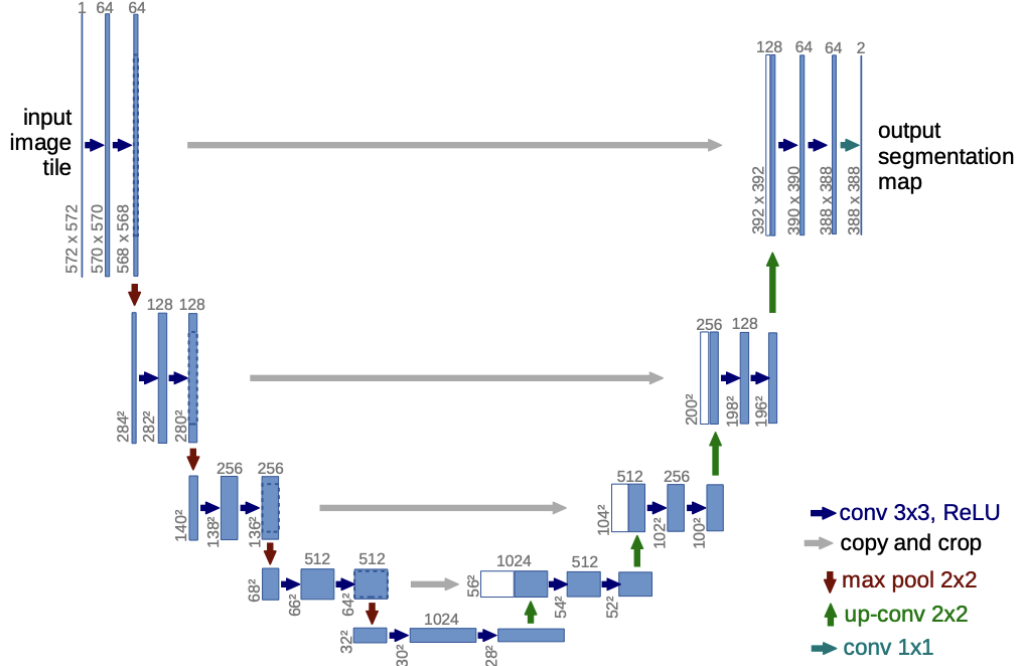


Figure 1: U-Net architecture for 32x32 pixels in the lowest resolution. Blue boxes are feature maps with the number of feature-channels on top of the boxes and the size shown on the left size. Operations are indicated by the arrows. The skip connections are a concatenation. The figure originally created by Ronneberger et al. [21].

The skip connections, connecting the different levels of encoder and decoder prevent a loss of information and extract the features at different resolutions to retrieve spatial information. By doing this, it is one of the first architectures to improve the classical FCNN for semantic segmentation [15]. While U-Net provides spatial localisation of features, its ability to generalise to multi-scale information is limited [18].

One restriction is that the input size must be chosen to apply all 2x2 max-pooling operations in the encoder to an even x and y size.

**LinkNet** Like U-Net, LinkNet consists of an encoder block for downsampling and a decoder block for upsampling. The downsampling is not done by max pooling as in the U-Net architecture but by using a stride of 2 in a convolutional layer. The initial encoder block also differs from the following blocks as it uses a larger kernel and max pooling. The decoder blocks upsample by a factor of 2 in each block. The final block differs again from the previous blocks. The main difference to the U-Net architecture is how the skip connections are used: Similarly to the U-Net, there are skip connections between the corresponding steps of the encoder and decoder, but the feature map from the encoder is not concatenated but added to decoder data. The LinkNet architecture is visualised in Figure 2. [4]

The implementation used in this project has four skip connections instead of the original three [11]. Similarly to the U-Net, the input size is restricted, so that every upsampling operation can be applied to an even x and y size.

LinkNet has been shown to achieve better results than U-Net under similar conditions [8].

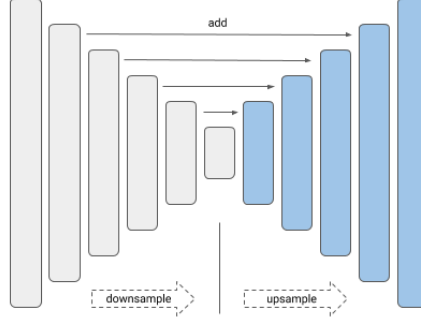


Figure 2: A visualisation of the LinkNet architecture originally provided by Iakubovskii [11].

**FPN** The Feature Pyramid Network (FPN) architecture creates feature maps of various sizes in multiple layers [18]. Like the other architectures, it consists of an encoder and a decoder, called bottom-up and top-down pathways here[14]. Similarly to U-Net, feature maps at different scales with a scaling step of 2 are created in the encoder [14]. In the decoder, the feature maps are upsampled and combined with the encoder information of the same level. Similarly to LinkNet, addition is used in the skip connections, but a  $1 \times 1$  convolution is applied. By doing this, so-called feature pyramids are built, containing features at different resolutions. Kirillov et al. proposed using these feature pyramids to obtain a segmentation by merging the feature maps using addition or concatenation [13, 11]. The architecture is visualised in Figure 3.

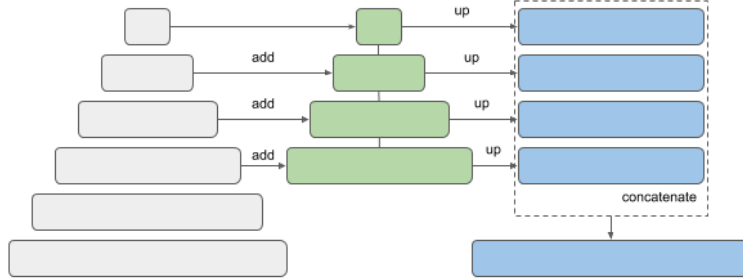


Figure 3: A visualisation of the FPN architecture originally provided by Iakubovskii [11]. Note, that the feature maps can be combined either by concatenation or addition.

**PSPNet** The central part of the Pyramid Scene Parsing Network (PSPNet) is the pyramid pooling module, visualised in part c of Figure 4, which extracts context information at different scales. A feature map extracted with a pre-trained backbone is pooled at different pyramid scales. This means that global pooling and sub-regions on different locations are used to extract features from a global to a more fine-grained scale. Each of those scales is passed through a  $1 \times 1$  convolution and afterwards upsampled to the size of the original feature map. All feature maps, including the original feature

map from the backbone, are concatenated and used to extract the final prediction. By this, features on different scales are combined. [24, 9]

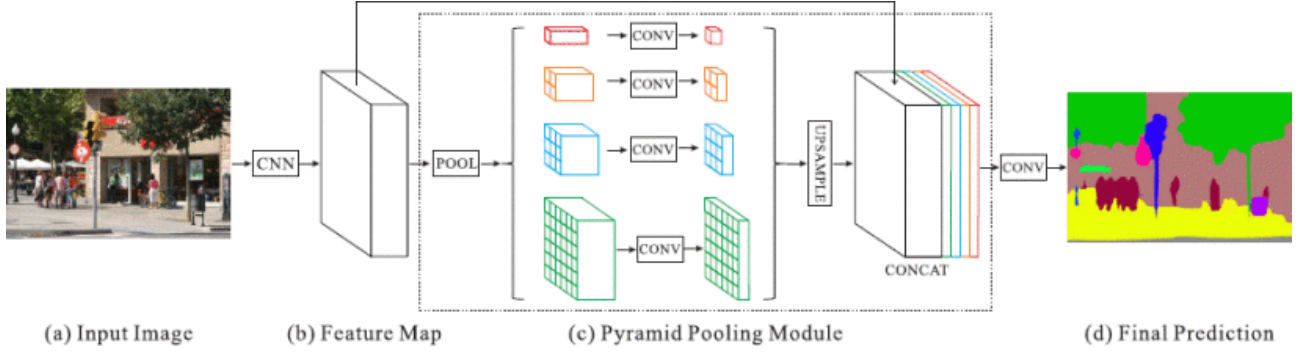


Figure 4: Visualization of the PSPNet-architecture. Originally created by Zhao et al. [24].

### 3.1.1 Optimisation and Evaluation

Several methods exist to evaluate how good a predicted segmentation is. Since semantic segmentation performs a pixel-wise classification, resulting in a segmentation mask, classical metrics such as accuracy and precision are available. Two performance metrics commonly used in semantic segmentation in medical imaging are the Dice Coefficient and the Intersection over Union (IoU) score. They indicate the segmentation quality better than pixel-wise accuracy [7].

**IoU-Score** The IoU-Score (Intersection over Union), also known as the Jaccard index  $J$ , describes the ratio between the intersection of the ground truth mask  $y$  and the predicted mask  $\tilde{y}$  and the union of the predicted and the ground truth mask. This compares the similarity of the two masks [5].

$$\text{IoU}(y, \tilde{y}) = \frac{\text{Area of overlap}}{\text{Area of union}} \quad (1)$$

$$= \frac{|y \cap \tilde{y}|}{|y \cup \tilde{y}|} \quad (2)$$

**Dice Coefficient** The Dice coefficient is the F1 score calculated for the image masks. Regarding intersection and union, it calculates the ratio between two times the overlap between ground truth  $y$  and predicted mask  $\tilde{y}$  and the total area.

$$\text{Dice}(y, \tilde{y}) = 2 \cdot \frac{\text{Area of overlap}}{\text{Total area}} \quad (3)$$

$$= 2 \cdot \frac{|y \cap \tilde{y}|}{|y| + |\tilde{y}|} \quad (4)$$

To gain more insight into the type of errors the model makes, the rate of false positives and false negatives can be reported and then used to differentiate Type I and Type II errors [12].

**Loss function** Although the Dice Coefficient and IOU-Score are the most commonly used evaluation metrics, pixel-wise cross-entropy is often used as a loss function [7]. Since it is shown that there is no direct link between pixel-wise cross-entropy, either weighted or not, and Dice Coefficient and IoU-Score, this choice does not make sense because it does not optimise towards the goal.

Differentiable approximations for Dice Coefficient and IoU-Score exist that can be used to perform more goal-orientated optimisation. Both metrics and loss functions are shown to be linked to each other [7].

### 3.1.2 Data Augmentation

Data Augmentation is a valuable technique to make trained models more robust and accurate. This is especially true if available data is limited, as the data set size can be increased or the data set can be made more diverse.

For images, there exist several different possible augmentations. First, there are different positional augmentations, including cropping, flipping, rotating and resizing the image. Another class of augmentations is colour augmentation, which changes the image's brightness, contrast or saturation. Other augmentations include blurring and dropouts.

Not every augmentation is appropriate for every application. Rotating images of standing animals by 180 degrees, for example, would not make sense, while the rotation of wound images is appropriate. Therefore, augmentations must be chosen carefully depending on the application.

## 3.2 Wound Segmentation

As already discussed in the motivation of this project, wound segmentation is a complex problem due to wound characteristics such as different tissues and, therefore, edges inside of a wound itself on one side and technical reasons such as, e.g. varying lightning, distance to the wound and different angles.

Before Deep Learning became easily accessible and popular, methods based on features describing colour and textures, region-growing with optimal thresholding algorithms, and classical machine learning models were used to perform segmentation [22]. Convolutional Neural Networks replaced manually extracted features with autonomously learned ones [22]. Some methods included pre-processing steps to remove the background by, e.g., user interaction indicating the background, using a standardized background when taking the image, or using manual feature engineering to detect the background more efficiently and make the wound segmentation task easier. Such non-automatic steps limit the use of the segmentation algorithms because they either require more resources in the image-taking process or the segmentation process or are specifically tailored for specific lighting conditions or camera settings.

The Diabetic Foot Ulcer Challenge 2022 used FCN, U-Net and SegNet with different backbones and categorical cross-entropy loss as the baseline for their challenge, indicating those methods reflect the current state of the art that needs to be improved [12]. Generally, such classic models are commonly

used and extended with minor adaptations. Two methods stood out in the performed literature review, including more sophisticated adaptations.

Scebba et al. proposed a method consisting of two steps: An object detection step that produces bounding boxes containing the wounds and a second step that performs segmentation on those areas. Segmentation is performed using classical architectures for semantic segmentation, as described in section 3.1. The loss function used was a pixel-wise weighted binary cross-entropy loss. Weighting was calculated based on the number of wound pixels and background pixels of each training set fold.

Oota et al. claim they set a new state of the art for wound segmentation while providing a data set together with their work [20]. The latter made them a suitable method for further investigation in this project's scope. Their approach is described in more detail in the following section.

### 3.2.1 WSNet

The framework proposed by Oota et al. uses the previously described segmentation architectures: U-Net, LinkNet, PSPNet, and FPN. Experiments with different backbones were performed in their work. However, in this project's scope, MobileNet [10] is mainly used since it is the smallest one, which allows faster training, which is needed in the limited time of the project.

ImageNet pre-trained weights are used. WSNet also describes pre-training specific to wounds, called Wound-Domain Adaptive Pre-training. During this pre-training, wound images are classified into five different ulcer types.

Oota et al. experimented with data augmentation on the training data and the corresponding masks, including optical distortion, horizontal flip, random rotation, blur, and more, to make their models more robust.

**Global-Local Architecture** The network architecture proposed by Oota et al. is called Global-Local architecture. It consists of two segmentation models, a global model and a local model, combining the result for the final segmentation. The global model is a standard segmentation model of one of the four architectures described in section 3.1. In the global model, the image (size  $192 \times 192 \times 3$ ) is split into 16 non-overlapping patches, resulting in a size of  $48 \times 48 \times 3$  per patch. The patches are then stacked, resulting in a size of  $48 \times 48 \times (3 \times 16)$ . The patches are the input to 16 local models in parallel, with shared weights between the local models. The output is eventually combined to obtain a full-sized mask. This mask and the output of the global model are concatenated to a mask of size  $192 \times 192 \times 2$ , and a final convolution of size  $1 \times 1$  results in the predicted mask. This architecture is motivated by the need to combine global signals from the entire image and local signals from smaller patches for more details. Only capturing local signals might cause an incomplete segmentation for large wounds. [20]

Although the combination of global and local signals sounds reasonable initially, it is interesting that this approach is combined with segmentation models that already contain different context sizes and localisation in these context sizes, as described in section 3.1. An explicitly chosen patch size implies some property of the wound images that makes this size particularly important for local information.



Oota et al. stated in their paper that they tested different patch sizes and chose 48 because it led to the best results [20], supporting the theory that this patch size yields more information than others.

**Reported Results** Oota et al. report that wound-specific pre-training improves the resulting segmentation. Furthermore, they find that data augmentation leads to improvements. As expected, the local-only models perform significantly worse than using the segmentation model as intended in a global way. Furthermore, they find that combining global and local models leads to an improved performance compared to the global models. This indicates that the chosen patch size yields valuable information for the segmentation. The best results are therefore achieved with wound-specific pre-training, data augmentation and the invented Global-Local architecture.

Reporting such results always leads to the question of whether they are reproducible. This is especially the case with the Global-Local architecture with a specific patch size, leading to questioning whether the patch size can be generalised to other image sizes and other data sets.

## 4 WSNNet

TODO: write introduction wanted to check results, first implement them, check for deviations, make experiments, look at explainability (maybe)

### 4.1 Code availability and reproduction of the results

Although the code for WSNNet [20] is stated to be publicly available, a closer inspection of the linked GitHub repository shows that this is only partially the case. A lack of documentation makes using the code hard, especially since it seems to contain multiple errors, making it only suitable as a base for new code.

In this project’s scope, the code was used to create runnable models again. Unfortunately, the classes of the wounds are not available, making it impossible to perform pre-training as described in the original paper [20]. In total, there are eight models available: A local model and a combined global-local model for each of the segmentation models: Unet, PSPNet, FPN, and LinkNet. The Python library used for the segmentation models is `segmentation_models` [11]. The implementation process showed some differences from the described model architecture. In particular, it was claimed that the wound images were split up in parts of 48px times 48px. However, three of the four models, all besides PSPNet, only allow input sizes divisible by 32, and the code in GitHub showed a size of 64px was used. Another difference between the available code and the paper is that it is claimed that augmentation is not performed on the test images, which is not the case.

Information about the training, validation and test set size is not given in the paper or code. However, the code reveals that the train and validation sets were just the first x% of the dataset, and no randomisation was used to separate the test set as it is usually done. In this project’s scope, a split of 70 % training, 15 % validation and 15 % test data is used.

Because the data training for the wound-specific pre-training is not available, the results can only be compared for imagenet pre-training.

- problem with imagenet pre-training with mobilenet: input size for patches is not available, instead the default size of 224 is used, which might impact results negatively

## 4.2 Comparison of the achieved performance

	Unet		LinkNet		PSPNet		FPN	
	IoU	Dice	IoU	Dice	IoU	Dice	IoU	Dice
<b>Local model</b>	0.359	0.523	0.398	0.564	0.373	0.538	0.408	0.574
<b>Global model</b>	0.504	0.668	0.631	0.772	0.458	0.627	0.632	0.772
<b>Global-Local model</b>	0.495	0.658	0.618	0.763	0.476	0.642	0.612	0.758

Table 1: IoU-Scores and Dice Coefficients for the four different models with each Global-Local, Global and Local architecture. The backbone used is mobilenet.

		U-Net		LinkNet		PSPNet		FPN	
		IoU	Dice	IoU	Dice	IoU	Dice	IoU	Dice
(A) Models with ImageNet pretraining	DenseNet121	0.617	0.761	0.617	0.762	0.585	0.736	0.623	0.766
	DenseNet169	0.613	0.758	0.624	0.768	0.596	0.745	0.614	0.760
	MobileNet	0.593	0.742	0.571	0.724	0.561	0.717	0.594	0.743
(B) Models with wound domain adaptive pretraining (WDAP)	DenseNet121	0.648	0.783	0.657	0.800	0.625	0.765	0.652	0.793
	DenseNet169	0.647	0.781	0.651	0.788	0.636	0.773	0.637	0.773
	MobileNet	0.615	0.760	0.611	0.755	0.563	0.718	0.616	0.758
(C) Models with WDAP and data augmentation	DenseNet121	0.680	0.818	0.687	0.820	0.653	0.797	0.680	0.817
	DenseNet169	0.672	0.810	0.675	0.812	0.656	0.801	0.664	0.807
	MobileNet	0.636	0.778	0.647	0.780	0.598	0.744	0.634	0.775
(D) Local (patch-based) models with WDAP	DenseNet121	0.527	0.689	0.537	0.698	0.520	0.682	0.532	0.694
	DenseNet169	0.534	0.696	0.530	0.691	0.519	0.681	0.533	0.696
	MobileNet	0.512	0.673	0.514	0.677	0.493	0.660	0.510	0.670
(E) Global-local models with ImageNet pretraining and data augmentation	DenseNet121	0.648	0.784	0.649	0.786	0.621	0.763	0.651	0.792
	DenseNet169	0.649	0.787	0.650	0.790	0.624	0.767	0.648	0.785
	MobileNet	0.620	0.761	0.621	0.763	0.565	0.722	0.618	0.760
(F) WSNET-FF: Global-local models with WDAP and data augmentation	DenseNet121	0.685	0.823	0.706	0.840	0.663	0.805	0.700	0.834
	DenseNet169	0.684	0.821	0.694	0.830	0.675	0.815	0.680	0.818
	MobileNet	0.650	0.790	0.651	0.792	0.590	0.740	0.651	0.792
(G) WSNET: Global-local models with WDAP, data augmentation, end-to-end fine-tuning	DenseNet121	0.695	0.831	<b>0.713</b>	<b>0.847</b>	0.683	0.820	<b>0.707</b>	<b>0.840</b>
	DenseNet169	<b>0.701</b>	<b>0.834</b>	0.707	0.841	<b>0.686</b>	<b>0.823</b>	0.697	0.832
	MobileNet	0.661	0.800	0.662	0.800	0.601	0.748	0.661	0.798

Table 2: Results reported by Oota et al. [20].

- results are comparable with results reported in paper, slightly lower scores
- e.g. Unet IoU score 0.495 with my code, 0.620 in paper (dice score 0.761 vs 0.658)
- others are closer (LinkNet 0.618 from me vs 0.621 in paper, dice 0.763 in paper and for me)
- maybe differences in training size
- most important thing: the global-local model does not improve about global model (or at least less than reported in paper)
- but they are still way more computationally expensive because you need to train two models instead of one

- as discussed before, an improvement indicates that something is going on with 48 px context size
- the results reported by Oota et al. are shown in figure

### 4.3 Experiments with the activation function

- code shows use of sigmoid as activation function
- literature of the model reports ReLU more frequently, thus it was tested as alternative to sigmoid
- no clear trend of one being clearly better for all models and architectures

### 4.4 Combination of different architectures

- used model architectures localize signals differently by design
- if the patch size really does play a significant role, maybe it makes sense to combine different architecture sizes?

## 5 Results and Evaluation

### 5.1 Re-implementation and evaluation of WNet

- contribution: reimplementation of a framework in a better documented way, making the reconstruction of results easier
- documentation of this implementation
- identified discrepancies between paper and available code
- comparison of results
- showed that reported "good" architecture does not yield significant performance improvements
- why: models already capture localized information, this is why those are sota segmentation frameworks, further localisation does not really make sense, maybe rather change parameters of used models to improve results
- Which architecture is suited best for wound segmentation? Why and what other alternatives would there be?

### 5.2 Robustness of wound segmentation

- augmentations commonly performed to improve robustness of models
- can also be used to assess robustness of the resulting model
- for clinical application, lighting and size might vary between images
- batch normalization might further increase this problem (TODO: search references)
-

### 5.3 Explainability of segmentation results

## 6 Technical Information

### 6.1 Code and Data Availability

The code produced in the project's scope is available on GitHub: <https://github.com/Zianor/DLIV-chronic-wound-segmentation>. Package versions are included to ensure reproducibility.

The used data is also available on GitHub: <https://github.com/subbareddy248/WSNET/> [19, 20]. Availability at a later point in time cannot be guaranteed.

### 6.2 Libraries

Several libraries were used in this project. All work is based on the Deep Learning framework TensorFlow with Keras [16, 6]. The implementation of the four used network architectures was provided by the Python library `segmentation_models` [11]. Image augmentations were performed with `Albumentations` [3].

### 6.3 Used Hardware

All computations are performed on a MacBook Air (24GB RAM, Apple M2 Chip with an 8-core GPU) or a computer with 16GB RAM and an Nvidia GeForce GTX 1070 Ti as GPU. The package versions for GPU-utilization on MacOS are included in the package versions on GitHub.

### 6.4 Prior Experience

I have a strong programming background, consisting of a B.Sc. in Computer Science and three years of experience in Web development with Python. Besides the Advanced Concepts of Machine Learning course, I have no experience with Deep Learning.

### 6.5 Learning Process

- Getting familiar with tensorflow
- learning about the state of the art in segmantic segmentation and segmentation of wound images and evaluation methods
- more experience in dealing with paper results and how trustworthy they are
- first, I planned on spending more time on the results of the chosen paper and experimenting with different augmentations and explainability
- after doing research about segmentation models I got sceptical about the general approach and spend a lot of time in researching semantic segmentation and the how and why
-

## References

- [1] Mohammad Faizal Ahmad Fauzi et al. “Computerized segmentation and measurement of chronic wound images”. In: *Computers in Biology and Medicine* 60 (2015), pp. 74–85. ISSN: 0010-4825. DOI: <https://doi.org/10.1016/j.compbiomed.2015.02.015>.
- [2] Vijay Badrinarayanan, Alex Kendall, and Roberto Cipolla. “SegNet: A Deep Convolutional Encoder-Decoder Architecture for Image Segmentation”. In: *IEEE Transactions on Pattern Analysis and Machine Intelligence* 39.12 (2017), pp. 2481–2495. DOI: 10.1109/TPAMI.2016.2644615.
- [3] Alexander Buslaev et al. “Albumentations: Fast and Flexible Image Augmentations”. In: *Information* 11.2 (2020). ISSN: 2078-2489. DOI: 10.3390/info11020125.
- [4] Abhishek Chaurasia and Eugenio Culurciello. “LinkNet: Exploiting encoder representations for efficient semantic segmentation”. In: *2017 IEEE Visual Communications and Image Processing (VCIP)*. 2017, pp. 1–4. DOI: 10.1109/VCIP.2017.8305148.
- [5] Yeong-Jun Cho. “Weighted Intersection over Union (wIoU): A New Evaluation Metric for Image Segmentation”. In: *ArXiv abs/2107.09858* (2021).
- [6] François Chollet et al. *Keras*. <https://keras.io>. 2015.
- [7] Tom Eelbode et al. “Optimization for Medical Image Segmentation: Theory and Practice When Evaluating With Dice Score or Jaccard Index”. In: *IEEE Transactions on Medical Imaging* 39.11 (2020), pp. 3679–3690. DOI: 10.1109/TMI.2020.3002417.
- [8] Yunya Gao et al. “Comparing the robustness of U-Net, LinkNet, and FPN towards label noise for refugee dwelling extraction from satellite imagery”. In: *2022 IEEE Global Humanitarian Technology Conference (GHTC)*. 2022, pp. 88–94. DOI: 10.1109/GHTC55712.2022.9911036.
- [9] *How PSPNet works?* URL: <https://developers.arcgis.com/python/guide/how-pspnet-works/> (visited on 12/16/2023).
- [10] Andrew G. Howard et al. *MobileNets: Efficient Convolutional Neural Networks for Mobile Vision Applications*. 2017. arXiv: 1704.04861 [cs.CV].
- [11] Pavel Iakubovskii. *Segmentation Models*. [https://github.com/qubvel/segmentation\\_models](https://github.com/qubvel/segmentation_models). 2019.
- [12] Connah Kendrick et al. *Translating Clinical Delineation of Diabetic Foot Ulcers into Machine Interpretable Segmentation*. 2022. arXiv: 2204.11618 [eess.IV].
- [13] Alexander Kirillov et al. “Panoptic feature pyramid networks”. In: *Proceedings of the IEEE/CVF conference on computer vision and pattern recognition*. 2019, pp. 6399–6408.
- [14] Tsung-Yi Lin et al. “Feature Pyramid Networks for Object Detection”. In: *Proceedings of the IEEE Conference on Computer Vision and Pattern Recognition (CVPR)*. July 2017.
- [15] Geert Litjens et al. “A survey on deep learning in medical image analysis”. In: *Medical Image Analysis* 42 (2017), pp. 60–88. ISSN: 1361-8415. DOI: <https://doi.org/10.1016/j.media.2017.07.005>.
- [16] Martín Abadi et al. *TensorFlow: Large-Scale Machine Learning on Heterogeneous Systems*. Software available from tensorflow.org. 2015.

- [17] Yujian Mo et al. “Review the state-of-the-art technologies of semantic segmentation based on deep learning”. In: *Neurocomputing* 493 (2022), pp. 626–646. ISSN: 0925-2312. DOI: <https://doi.org/10.1016/j.neucom.2022.01.005>.
- [18] Abderrahim Norelyaqine, Rida Azmi, and Abderrahim Saadane. “Architecture of deep convolutional encoder-decoder networks for building footprint semantic segmentation”. In: *Scientific Programming* 2023, 8552624 (2023). DOI: <https://doi.org/10.1155/2023/8552624>.
- [19] Subba Reddy Oota et al. “HealTech - A System for Predicting Patient Hospitalization Risk and Wound Progression in Old Patients”. In: *Proceedings of the IEEE/CVF Winter Conference on Applications of Computer Vision (WACV)*. Jan. 2021, pp. 2463–2472.
- [20] Subba Reddy Oota et al. “WSNet: Towards an Effective Method for Wound Image Segmentation”. In: *Proceedings of the IEEE/CVF Winter Conference on Applications of Computer Vision (WACV)*. Jan. 2023, pp. 3234–3243.
- [21] Olaf Ronneberger, Philipp Fischer, and Thomas Brox. “U-Net: Convolutional Networks for Biomedical Image Segmentation”. In: (May 2015).
- [22] Gaetano Scebba et al. “Detect-and-segment: A deep learning approach to automate wound image segmentation”. In: *Informatics in Medicine Unlocked* 29 (2022), p. 100884. ISSN: 2352-9148. DOI: <https://doi.org/10.1016/j.imu.2022.100884>.
- [23] Chuanbo Wang et al. *Fully automatic wound segmentation with deep convolutional neural networks*. en. Dec. 2020. DOI: 10.1038/s41598-020-78799-w.
- [24] Hengshuang Zhao et al. “Pyramid Scene Parsing Network”. In: *2017 IEEE Conference on Computer Vision and Pattern Recognition (CVPR)*. 2017, pp. 6230–6239. DOI: 10.1109/CVPR.2017.660.